STUDY ON HEAT TRANSFER PERFORMANCE OF SPIRAL FIN PLATE COLLECTOR

Ying Xu, Jingyi Shi*, Zhuangzhuang Ren, Xiaoyan Liu, Xin Nie

School of Mechanical Science and Engineering, Northeast Petroleum University, Daqing 163318, China

*Corresponding author: sjybb23101@163.com

As an important equipment for solar thermal utilization, solar collector is the key to improve energy efficiency and reduce carbon emissions. However, in order to improve the heat transfer capacity of solar collectors, further optimization of their design and performance is the focus of current research. Although the addition of traditional ribs strengthens the lateral air flow, it also increases the heat transfer cavity between the heat transfer mass and the heat absorbing plate. Therefore, in this paper, a new spiral finned flat plate collector is designed from the perspective of the synergistic flow of the heat exchanger mass in the transverse and longitudinal directions. The flow and heat transfer mathematical model of the new collector is established, and numerical simulations are carried out to analyze the effects of the ribbed deflector width and spiral pitch on the collector efficiency. The results show that the heat transfer capacity of the new collector is significantly higher than that of the flat plate collector. In addition, for the spiral rib with a rib height of 38 mm and a diameter of 25 mm, the optimal deflector width is 16 mm, the spiral pitch is 160 mm, and the deflector angle is 33.92°.

Keywords：*spiral ribs; strengthen heat transfer; structural optimization; horizontal and vertical collaborative diversion*

1.Introduction

Against the background of global climate change and increasingly severe energy crisis, it has become a consensus among countries to promote the development and application of clean energy technologies [1,2]. The consumption of traditional fossil energy has not only led to a large amount of greenhouse gas emissions, but also caused far-reaching impacts on the ecological environment [3,4]. In order to realize sustainable development, countries have set targets to reduce carbon emissions and accelerated the pace of transitioning to low-carbon and zero-carbon energy systems [6,7]. In this process, solar energy, as a clean, renewable and inexhaustible energy source, has attracted much attention [8]. Solar collectors are widely used for heating, drying, and building heating because of their ability to efficiently convert solar radiant energy into thermal energy [9]. However, conventional solar flat-plate air collectors have low thermal conversion efficiency (<40%), and there is an urgent need to improve their thermal efficiency and reduce the cost by optimizing the structural design, upgrading the

material properties, and improving the fluid flow method [10].

Many scholars have strengthened the degree of heat exchange between the heat absorbing plate and the air by adding fins. Kumar et al. [11] set up discrete W-shaped fins in the FPC and studied its heat transfer performance (HTP) experimentally, indicating that the work performance can be improved by 2.16 times compared to the ordinary FPC. Saini et al. [12] investigated the influence of arc fins on the performance parameters (heat transfer and friction coefficient) of the collector. The study indicated that the heat transfer coefficient (HTC) of the fin with an arc of 0.333 can be increased by 3.6 times. Liu et al. [13] conducted a numerical simulation of the collector with L-type fins, finding that the instantaneous heat transfer efficiency is significantly improved, and the effect of rib height on heat collection capacity is positively correlated. Chaube et al. [14], Y Yadav et al. [15], and Bhagoria et al. [16] numerically simulated the effects of three kinds of fins (metal wire transverse fins, square transverse fins, triangular transverse fins) on the heat transfer and flow between air and collector are numerically simulated. It is found that the average Nusselt number is negatively correlated with the relative rib spacing and positively correlated with the rib height. Tanda et al. [17] used liquid crystal thermal imaging experiments to study the influence of fin continuity on the HTP in a rectangular channel, finding that the shape and geometry of the ribs have a significant impact on the HTC. Machi M. H. et al. [18] experimentally studied a solar air collector (SAC) with triangular fins, showing that a greater temperature difference between the inlet and outlet of the finned collector results in higher effective heat. It showed that the greater the temperature difference between the inlet and outlet of the collector with fins, the higher the effective heat. Fahmi et al. [19] experimentally analyzed the energy conversion rate of an SAC with triangular fins, finding that these fins could effectively improve the thermal performance (TP) of the SAC without increasing flow resistance. Promth et al. [20] applied 30° angle corrugated triangular ribs to an FPC and found that these ribs reduced the thermal boundary layer thickness, increased turbulence, and enhanced heat transfer. From the above cases, it is evident that the shape of the ribs significantly affects the heat transfer performance of the collector.

Currently, research on collectors with V-shaped ribs is more extensive. Zhang M [21] et al. simulated the HTP of an absorber plate collector with V-shaped fins. They found that as air flows through the channel, it produces vortices and spirals forward, leading to more thorough air mixing and improved heat transfer of the absorber plate. El-Sebaii et al. [22] evaluated the thermal performance of a double-finned flat-plate SAC both experimentally and theoretically, comparing the effects of using V-shaped corrugated plates or ribs in the channel. The results showed that the dual-channel V-shaped corrugated plate air collector exhibits higher efficiency. Singh et al. [23] experimentally studied the effect of V-shaped fin roughness on the heat transfer performance of a solar collector and identified the optimal fin roughness. Jiang et al. [24] transformed a V-shaped fin perforation into a V-shaped perforated plate permeable flat plate collector, and simulated as well as experimentally studied its thermal efficiency. The results revealed that the thermal efficiency of the V-shaped perforated plate solar collector is 3.73% ~ 24.89% higher than that of the traditional flat plate collector (TFPC). Liu et al. [25] modified multiple V-shaped ribs to create a new type of S-shaped rib and analyzed the influence of rib structure on the TP of the collector through both experiments and simulations.

The results indicated that the gap in the S-shaped fin can improve heat collection efficiency (HCE) by reducing airflow resistance. From the above study, the addition of V-shaped ribs causes the air to swirl and spiral forward in the flow, leading to better air mixing and enhanced heat exchange with the heat-absorbing plate. However, while heat transfer efficiency improves, airflow resistance and heat transfer cavities also increase, preventing further improvement in the overall efficiency of the flat plate collector.

In summary, the shape of the ribs significantly affects the efficiency of the collector in medium- and high-temperature heat transfer channel structures. Although the addition of traditional ribs strengthens transverse airflow, it also increases the heat transfer cavity between the heat transfer medium and the heat-absorbing plate. Therefore, this paper designs a new spiral finned flat plate collector based on the concept of synergistic transverse and longitudinal heat exchanger flow. This structure effectively reduces heat transfer cavities, increases the heat transfer area, and extends heat transfer time, thereby further improving the collector's efficiency. A physical heat transfer model of the collector was established, and numerical simulations were conducted to analyze the effects of the ribbed deflector width and helical pitch on the collector's efficiency, ultimately determining the optimal structural parameters of the ribbed plate.

2. Modeling

2.1. The SPFC design

The heat-absorbing plate is a key component of a flat plate collector for light-to-heat conversion, and its structural design is crucial for influencing the flow of the heat transfer medium and overall heat transfer efficiency. In existing flat plate collectors, ribs are primarily designed for lateral infusion, which causes the air flowing through the heat transfer channel to create heat transfer cavities, leading to insufficient heat transfer between the air and the surface of the heat-absorbing plate. Additionally, most of the heat from the heat-absorbing plate is transferred to the material directly beneath it, while the heat-exchanging material farther away receives less heat and exits the channel. This results in inefficient and uneven heat transfer across the entire heat-exchanging channel. Therefore, this paper designs a spiral ribbed collector with a deflector to study the enhanced heat transfer characteristics of the collector under the influence of transverse and longitudinal synergistic flow in a high heat transfer channel, aiming to achieve efficient and uniform heat transfer.

According to Fig. 1, the overall size of the collector is 1010 mm × 590 mm × 105 mm, which mainly consisted of a heat absorbing plate, transparent cover plate, spiral guide fins, insulation layer, and shell. The size of the glass cover plate is 1010 mm×590 mm×5 mm, and the material is PC low iron glass. Its transmittance is as high as 0.91, which can penetrate a large amount of solar radiation. The overall size of the heat absorbing plate is 1000 mm×500 mm×5 mm, whose surface is connected with a crisscross arrangement of spiral guide fins. The purpose is to increase the contact area between the heat-absorbent surface and the air and boost the degree of turbulence. The spiral guide fin structure is a central cylindrical side surface connected to two guide components with downwind spiral and leeward spiral guide sheets. The spiral fin structure is shown in Fig. 2. The main purpose is to fully mix the heat-exchanged air with the unheated air to achieve efficient and uniform heat transfer. Both

the heat absorbing plate and fins are made of aluminum-zinc plate. The surfaces are coated with high-performance black chromium magnetron sputtering selective heat absorbing coating. The absorption rate is 0.92, and the infrared emissivity is only 0.06. The bottom and surrounding of the heat absorbing plate are surrounded by a glass wool insulation layer with excellent thermal insulation effect, and the outermost layer is fixed with an aluminum shell to secure the collector. The air inlet and outlet are installed on both sides of the collector.

The meaning of the rib symbol is shown in Tab.1. The rib structure parameters designed in this paper mainly consider the rib height h and the diversion angle θ. The formula of the diversion angle θ is:

$$\theta = 90° - \arctan\frac{S}{\pi d} \tag{1}$$

The guide vanes involved are mainly double-thread, and the structural parameters of the spiral fins are shown in Fig. 2. According to the definition of double-thread lead, the lead of double-thread is equal to 2 times the pitch of the spiral (S = 2p). Therefore, the main structural parameters of the spiral guide rib are the height of the rib, the diameter of the spiral, the width of the guide plate, and the pitch of the spiral.

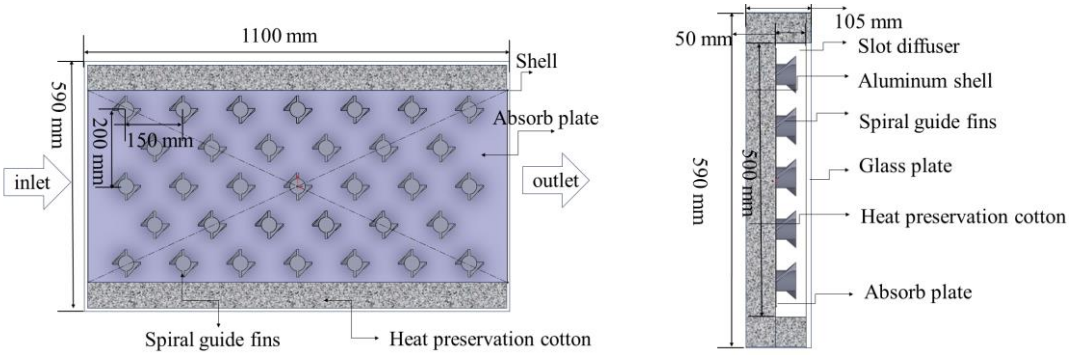

Fig. 1. Main view of structure design of spiral finned plate collector

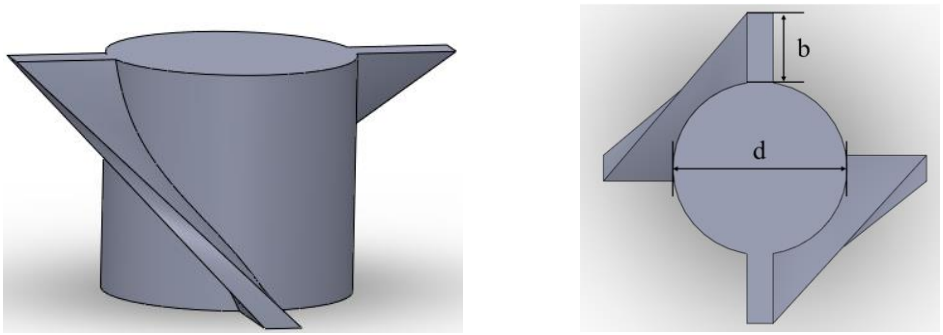

Fig. 2. Structure of fins

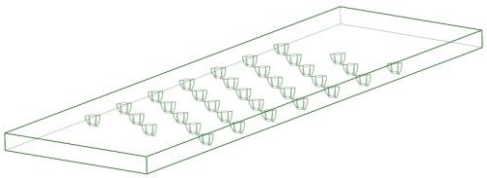

Fig. 3. Collector model

2.2. Research method

2.2.1. Mathematical model

This work mainly studies the influence of the geometric size of the fins on the HTP of the collector. Since the heat transfer of air inside the model is extremely complicated, the following assumptions are made for it to facilitate processing:

1. Heat loss at the inlet and outlet is ignored;
2. The glass plate and the external environment are mainly convection and radiation heat transfer;
3. The air flow process is steady-state flow;
4. The heat flux density of the heat-absorbing plate is constant;
5. Air is an incompressible ideal fluid.
6. The boundary conditions of the model are set as shown in Tab. 1.

The governing equations involved in the airflow in the FPC are as follows:

Continuity equation [26]:

$$\frac{\delta\rho}{\delta t}+\frac{\delta(\rho u)}{\delta x}+\frac{\delta(\rho v)}{\delta y}+\frac{\delta(\rho w)}{\delta z}=0 \tag{2}$$

Momentum conservation equation [27]:

$$f_x-\frac{1}{\rho}\frac{\delta p}{\delta x}+\frac{\mu}{\rho}\left(\frac{\delta^2 u}{\delta x^2}+\frac{\delta^2 u}{\delta y^2}+\frac{\delta^2 u}{\delta z^2}\right)=\frac{\delta u}{\delta t}+u\frac{\delta u}{\delta x}+v\frac{\delta u}{\delta y}+w\frac{\delta u}{\delta z} \tag{3}$$

$$f_y-\frac{1}{\rho}\frac{\delta p}{\delta y}+\frac{\mu}{\rho}\left(\frac{\delta^2 v}{\delta x^2}+\frac{\delta^2 v}{\delta y^2}+\frac{\delta^2 v}{\delta z^2}\right)=\frac{\delta v}{\delta t}+u\frac{\delta v}{\delta x}+v\frac{\delta v}{\delta y}+w\frac{\delta v}{\delta z} \tag{4}$$

$$f_z-\frac{1}{\rho}\frac{\delta p}{\delta z}+\frac{\mu}{\rho}\left(\frac{\delta^2 w}{\delta x^2}+\frac{\delta^2 w}{\delta y^2}+\frac{\delta^2 w}{\delta z^2}\right)=\frac{\delta w}{\delta t}+u\frac{\delta w}{\delta x}+v\frac{\delta w}{\delta y}+w\frac{\delta w}{\delta z} \tag{5}$$

Energy conservation equation [28]:

$$\lambda\frac{\delta^2 T}{\delta x^2}+\lambda\frac{\delta^2 T}{\delta y^2}+\lambda\frac{\delta^2 T}{\delta z^2}=c_p\left[\frac{\delta T}{\delta t}+\frac{\delta(uT)}{\delta x}+\frac{\delta(vT)}{\delta y}+\frac{\delta(wT)}{\delta z}\right]+S \tag{6}$$

Tab.1 Boundary condition setting

Boundary name	Boundary condition type	parameter setting
The bottom surface of heat absorbing plate	Constant heat flow	Q=569W/m^2
The upper surface of the glass	Mixed boundary conditions	13.3W/(m^2·K)
Surface of fins and heat-absorbing plate	Fluid-solid coupling	—
Bottom and side	Adiabatic	Q=0
Air inlet	Speed entrance	—
Air outlet	Pressure outlet	—

Turbulence model:

In this paper, A model is used as the turbulence model of fluid. Due to the limitations of the k-ε model, the enhanced wall function is used near the wall surface [29].

The k equation and ε equation in the RNG k-ε model are [30]:

$$\begin{aligned}\frac{\delta(\rho k)}{\delta t}+\frac{\delta\left(\rho k u_i\right)}{\delta x_i}&=\frac{\delta\left[\alpha_k \mu_{eff}\frac{\delta k}{\delta x_j}\right]}{\delta x_j}+G_k+\rho\varepsilon\\ \frac{\delta(\rho\varepsilon)}{\delta t}+\frac{\delta\left(\rho\varepsilon u_i\right)}{\delta x_i}&=\frac{\delta\left(\alpha_\varepsilon u_{eff}\frac{\delta\varepsilon}{\delta x_j}\right)}{\delta x_j}+\frac{C_{I\varepsilon}\varepsilon}{k}G_k-C_{2\varepsilon}\rho\frac{\varepsilon^2}{k}\end{aligned} \tag{7}$$

Radiation model:

Due to the large temperature difference between the absorber plate and the glass cover plate, the radiation heat transfer in the collector cavity needs to be considered. The radiation heat transfer between the glass cover plate and the heat absorbing plate adopts the DO model. [29]. The formula is as follows：

$$q=\lambda\delta(T_1^4-T_2^4) \tag{8}$$

The combined TP factor is calculated as follows:

Increasing the heat transfer rate of a heat absorbing plate by adding ribs to the plate is accompanied by an increase in the surface frictional resistance factor. Therefore Dewitt [31] proposed a parameter that can significantly increase the heat transfer performance of the heat absorbing plate to air without increasing the friction resistance factor too much, i.e., the overall evaluation of the TP of the air collector by the ratio of the convective heat transfer performance to that of the smooth flat plate collector：

$$\varepsilon=\frac{\bar{N}u}{\bar{N}u_x}\left(\frac{f}{f_x}\right)^{\frac{1}{3}} \tag{9}$$

where $\bar{N}u$ denotes the average Nu of convective heat transfer for a collector with sur face roughness; f denotes the frictional resistance factor for a collector with ribs; $\bar{N}u_x$ ($\bar{N}u_x=0.023Re^{0.8}\,\mathrm{Pr}^{0.4}$)denotes the average Nu of convective heat transfer for a s mooth flat plate collector; and f_x ($f_x=0.081Re^{-0.25}$)denotes the frictional resistance f actor for a smooth flat plate.

2.2.2. Grid independence verification

The tetrahedral unstructured grid was used to mesh the collector with h = 38, d = 20, w = 16, p = 160 fin structure. The boundary layer was divided on the surface of the fin and the heat-absorbing plate, and the local refinement was carried out. At the same time, the Nusselt number Nu was used as a measure to verify the independence. The grid independence verification results are shown in Tab. 2.

Tab. 2 Grid independence verification

Maximum mesh size (mm)	Number of grids (tens of thousands)	Nusselt number (Nu)	relative error
12	112.8435	52.60	-
10	281.8579	55.98	6.03%
7	634.3850	56.66	1.19%

As shown in Tab. 2, when the number of grids exceeds 281.8579 million, the Nusselt number gradually decreases with the increase in the number of grids, and the relative error is less than 2%. At this time, the number of grids has little effect on the calculation results. Therefore, in this paper, the maximum grid size is 10 mm, the minimum grid size of the boundary layer is 4 mm, the boundary layer thickness is 0.2 mm, the growth rate is 1.2, and the number of layers is 10 layers. A detailed view of the mesh is given in Fig. 4.

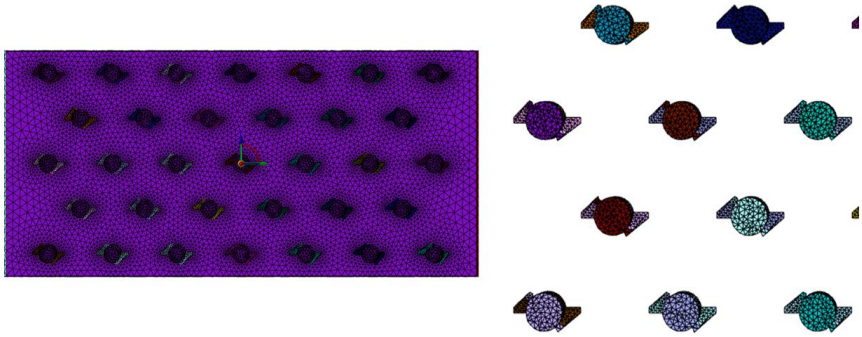

Fig. 4. Grid display

2.2.3. Material physical parameters

The airflow in the collector is more complicated due to the disturbance of the fins, so the airflow is forced airflow. Therefore, in the simulation process, it was considered that the air is an incompressible ideal gas, and the air does not absorb solar radiation. The material parameters of the collector components are shown in Tab. 3, and the air physical parameters are shown in Tab. 4.

Tab. 3 Collector component material parameter

	Shell	Glass	Glass wool	Heat absorbing plate
Density (kg/m^3)	2719	2230	120	2790
Specific heat capacity (J/(kg·K))	871	900	660	890
Thermal conductivity(W/(m·K))	202.4	1.2	0.035	202.4
Absorption rate	—	0.01	—	0.96
Internal emissivity	—	0.89	—	0.09
Transmittance	—	0.92	—	—
Refractive index	—	1.1	—	—

Tab. 4 Air physical parameters

Property	unit	value
Density	kg/m^3	—
Specific heat capacity	J/ (kg · K)	1006.43
Thermal conductivity	W/ (m · K)	0.0242
Viscosity	kg/ (m · s)	1.8×10^{-5}

2.3. Comparison of collector types

It is verified that the spiral fin designed in this paper has higher heat transfer efficiency for the collector. In this paper, Fluent numerical simulation was carried out on the spiral fin collector, cylindrical fin collector, and ordinary flat plate collector with the same size specifications and material parameters under the same working conditions. The performance of the three collectors was compared by parameters such as the wall temperature of the heat-absorbing plate, the convective HTC, and the HCE. The collector performance comparison is shown in Tab. 5.

Table 5 Collector performance comparison table

	Average convective HTC W/(m^2 • K)	Average wall temperature（K）	HCE
Ordinary flat plate collector	7.5	373.8	37.8%
Cylindrical fin collector	11.3	339.9	58.6%
Spiral fin collector	15.6	324.1	65.2%

As shown in Tab. 5, the new spiral fins can enhance the HTP of the collector. Among them, the heat-absorbing plate changes from no ribs to ribs (cylindrical ribs) the average temperature of the wall is reduced by 9.06%, the average convective HTC is increased by 33.12%, and the HCE is increased by 20.74%, which indicates that the existence of the fins will greatly improve the HCE of the collector. When the absorber plate is changed from a cylindrical fin to a spiral fin, the average wall temperature is reduced by 4.64%, the average convective HTC is increased by 27.38%, and the HCE is increased by 6.64%, which indicates that the heat transfer effect of the spiral fin plate collector is stronger.

3. Numerical Simulation Results and Analysis

The spiral fins can greatly enhance heat transfer intensity in the air channel but also increase the airflow resistance, which seriously affects the HTP of the collector. In this paper, based on the analysis of the influence of different rib structure parameters (guide vane width, spiral pitch) on the HTP of the collector, the surface temperature of the heat absorbing plate was compared by numerical simulation. The influence of spiral fins on the comprehensive performance of the collector is discussed, and the structural parameters of the spiral fins were optimized.

3.1 The influence of deflector width on the HTP of the collector

Under the condition that the rib height was 38 mm, the rib diameter was 25 mm, and the

spiral pitch of the deflector was 160 mm, the HTP of the collector was studied when the width of the deflector was 12 mm, 16 mm, 20 mm, and 24 mm, respectively.

Fig.4 (a ~ d) showed the temperature distribution of the collector with fins of different deflector widths at the air inlet velocity of 0.75 m/s.

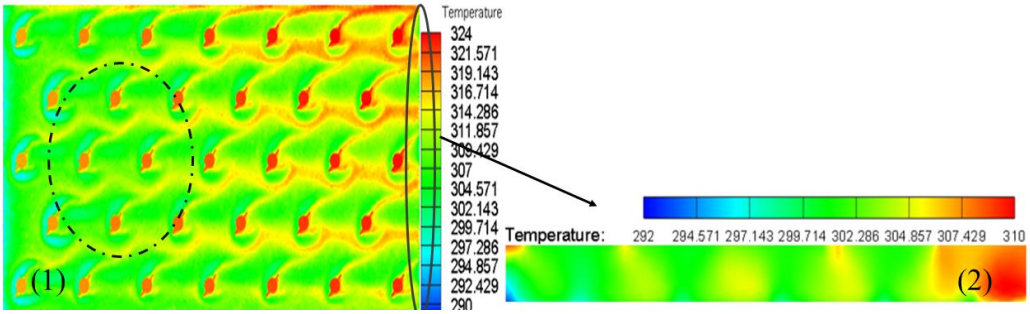

a. The temperature distribution of the collector with deflector widths of 12 mm

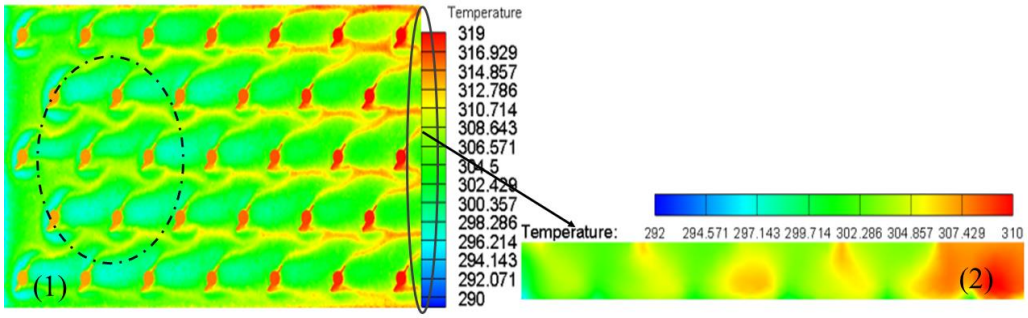

b. The temperature distribution of the collector with deflector widths of 16 mm

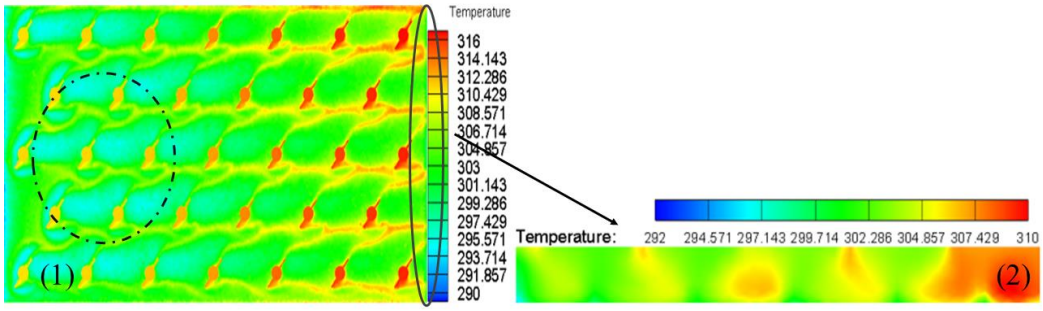

c. The temperature distribution of the collector with deflector widths of 20 mm

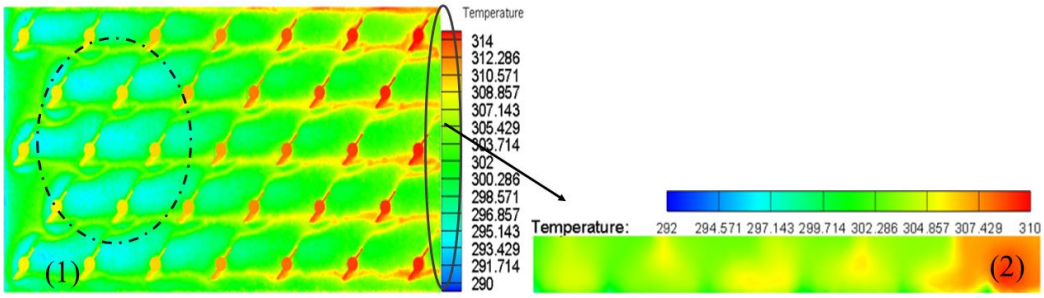

d. The temperature distribution of the collector with deflector widths of 24 mm

Fig.5. The temperature distribution of the collector with fins of deflector widths

Fig.5 (a (1) ~ d (1)), illustrated that the width of the guide vane was negatively correlated with the average temperature of the wall surface of the heat-absorbing plate. The width of the

deflector was proportional to the flow rate, and the smaller the width of the deflector, the less the damage to the wall boundary layer, so the overall temperature of the heat-absorbing plate was higher. With the increase in the width of the guide vane, the airflow channel heat transfer continuously enhanced, and the low-temperature region increased gradually. From the overall perspective, as the width of the guide vane gradually increased, the surface temperature distribution of the heat-absorbing plate was more uniform, and the heat transfer was better.

In Fig. 5 (a (2) ~ d (2)), the highest temperature at the outlet of the collector was also on the right side of the outlet, and its area increased first and then decreased with the increase in the width of the guide vane. The small area of low temperature on the left side gradually decreased until it disappeared. As the width of the guide vane increased, the temperature around the rib increased. This is because the wider the guide vane, the greater the damage to the wall boundary layer. Moreover, the wider guide vane would introduce more fully heat-exchanged air into the upper part of the fin, which helped to strengthen the heat exchange of air with insufficient heat transfer. The air temperature gradually increases along the flow direction, which leads to a decrease in temperature difference and a decrease in heat transfer. The heat transfer capacity of the outlet of the collector is weakened.

Fig.6 (e ~ h) shows the internal airflow diagram of the collector at the stage of full development of airflow with an airflow rate of 0.75 m/s and an air channel height of 20mm under different widths of the deflector.

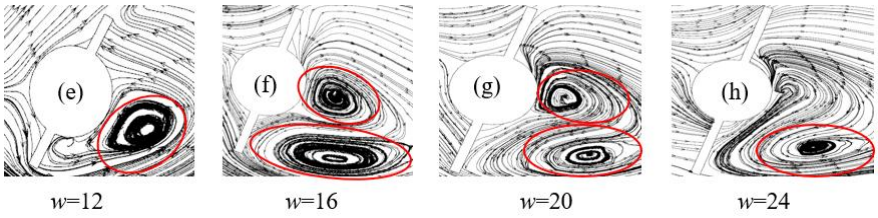

Fig.6 The internal air streamline diagram of the collector under different widths of the deflectors

Fig. 6 illustrates that in the stage of full airflow, as the width of the deflector increased, the vortex behind the fin became a larger vortex. The streamline density gradually became sparse, and then the vortex began to shrink and gradually moved away from the wall. When the width of the guide vane was 16 mm, the streamline density was closest to the fin wall, the impact force was the largest, and the degree of airflow disturbance was the strongest. As the width continued to increase to 20 mm and 24 mm, the vortex gradually moved away from the fins, the impact force decreased, and the degree of airflow disturbance decreased.

The change of the CTPF of the collector with the width of the deflector at different flow rates is shown in Fig.6.

As the inlet flow rate increased, the CTPF of the collector decreased continuously. With the increase in air inlet velocity, the spiral fin with the guide vane width w=12 mm had a small air flow rate, which could not achieve uniform heat transfer, and the CTPF was the smallest. Among the selected deflector widths, the collector with a width of 16 mm had the largest CTPF. While achieving full turbulence heat transfer uniformity, the flow loss was relatively small, resulting in the largest CTPF. Therefore, the width of the guide vane selected in this section was 16 mm.

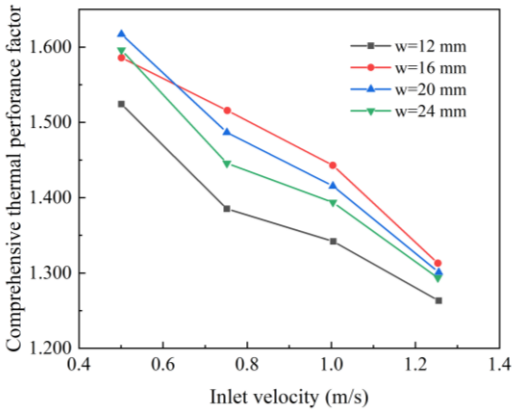

Fig. 7 Changes of comprehensive performance factors of collectors at different flow rates

3.2 The influence of guide vane pitch on the HTP of the collector

Under the conditions of rib height of 38 mm, rib diameter of 25 mm, and guide vane width of 16 mm, the HTP of the collector with different guide vane pitches (160 mm, 210 mm, 260 mm, and 310 mm) was investigated.

Fig.8 (a ~ d) showed the temperature distribution of the collector with fins of different pitch widths at the air inlet velocity of 0.75 m/s.

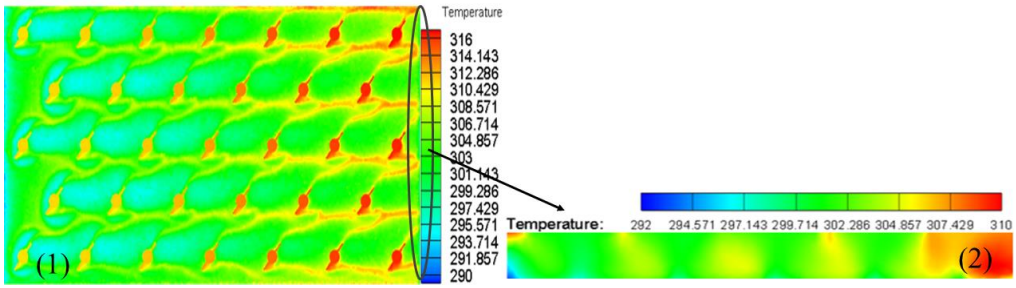

a. The temperature distribution of the collector with guide vane pitches of 160 mm

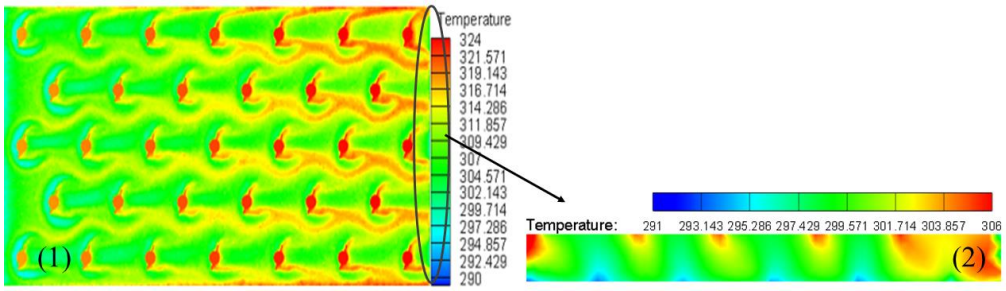

b. The temperature distribution of the collector with guide vane pitches of 210 mm

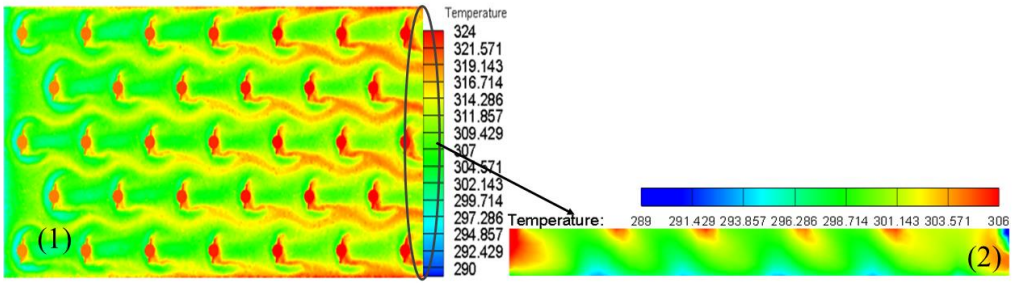

c. The temperature distribution of the collector with guide vane pitches of 260 mm

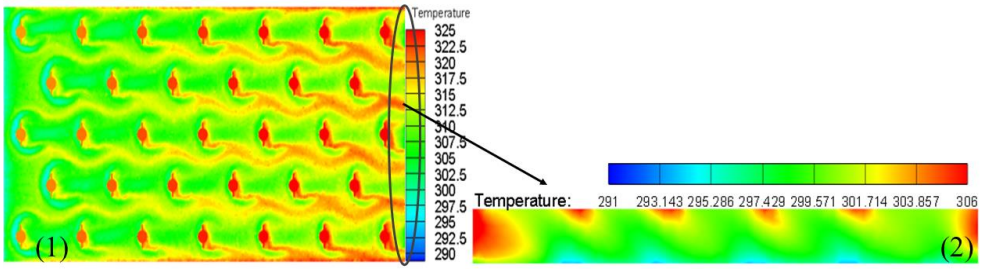

d. The temperature distribution of the collector with guide vane pitches of 310 mm

Fig. 8 The temperature distribution of the collector with fins of different guide vane pitches

Fig. 8 (a1 ~ d1) illustrates that the wall temperature of the absorber plate increases with the increase in the pitch of the guide vane, the area of the high-temperature area on the right side (especially on the lower right side), and the temperature around the fin also increased. The surface temperature of the heat-absorbing plate was the lowest when the pitch of the deflector was 160 mm, and the change was not obvious under other parameters. Therefore, when the pitch was greater than 210 mm, it did not affect the heat transfer effect.

It can be seen from Fig. 8 (a (2) ~ d (2)) that the temperature on the right side of the outlet decreased, while the temperature on the left side increased and the range became larger. The temperature in the area above the fin also increased gradually. This was because the increase in the helical pitch made the diversion angle of the guide vane smaller and the amount of air diversion smaller, which resulted in a small amount of heat-exchanged air entering the upper part of the fin, and the air in the heat exchange channel could not achieve fully uniform heat transfer. As the heat-exchange air continued to flow, the temperature difference in the heat exchange channel decreased, resulting in weak heat transfer on the right side of the collector. At the same time, the transverse flow direction of the fins was changed, resulting in more insufficient heat transfer to the upper right side, so the heat transfer in the upper right side was stronger than that in the lower right side.

Fig. 9 (e ~ h) was the airflow line diagram inside the collector at the stage of full development of airflow under different guide vane pitches when the height of the airflow channel was 20 mm.

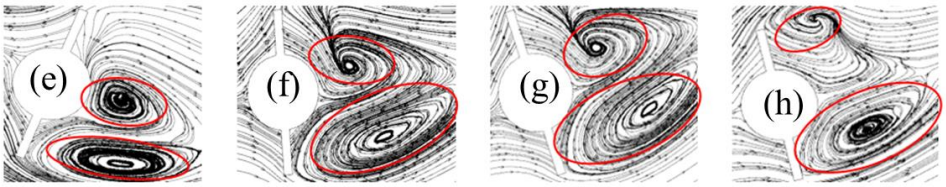

Fig. 9 The internal air streamline diagram of the collector under different pitches of the deflectors

It can be seen from Fig. 9 that as the spiral pitch of the guide vane increased, the spiral angle of the guide vane rotated counterclockwise, and the double vortices behind the ribs gradually moved away from the ribs, resulting in a decrease in impact on the wall surface. The degree of turbulence of the vortex to the air also decreased, and the HTP began to deteriorate. When the helical pitch was greater than 210 mm, the streamline flow angle flowed towards the upper right

of the heat exchange channel. Combined with Fig. 8, it can be seen that the HTP on the upper right side of the heat-absorbing plate was stronger than that on the lower right side, and the high-temperature area on the exit left increased.

The change of the CTPF of the collector with the width of the deflector at different flow rates is shown in Fig.10.

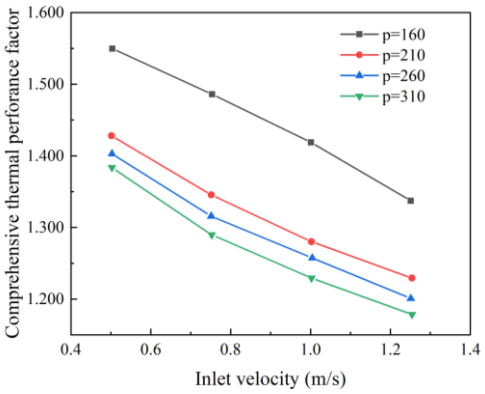

Fig. 10 The change of CTPF of collector under different inlet flow rates

From Fig. 10, it can be seen that the CTPF is negatively correlated with the change in the inlet flow rate. In the selected spiral pitches of the guide vane, when the spiral pitch was 160 mm, 210 mm, 260 mm, and 310 mm, the diversion angles were 33.92°, 10.55°, 9.23°, and 7.26°, respectively. When the spiral pitch was greater than 210 mm, the diversion angle of the guide vane was not much different. The diversion angle for the spiral pitch of 160 mm was much larger than the other diversion angles, and the air conduction flow was the largest, and the air could fully and evenly transfer heat. Therefore, the CTPF of the collector with a spiral pitch of 160 mm was the largest, so the spiral pitch of the guide vane selected in this section was 160 mm.

4.Conclusions

In this paper, an FPC with spiral guide fins was designed, its physical and mathematical models were established, and numerical simulation and analysis were implemented. Based on the research results of the effect of different fin structure parameters on the HTP of the collector, the structure was optimized and designed. The important conclusions are as follows:

(1) In this paper, numerical simulation and comparative analysis of ordinary, cylindrical fins, and spiral fins were carried out under the same working conditions. The performance of the collector with cylindrical fins was better than that of the TFPC, and the average wall temperature of the new spiral fin absorber plate was 4.64% lower than that of the cylindrical fin absorber plate. The average convective HTC increased by 27.38%, and the HCE increased by 6.64%. Therefore, the new spiral fins can effectively improve the HTP of the collector.

(2) In the heat exchange channel of the spiral fin flat plate collector designed in this paper, secondary flow and double vortices were generated behind the fins, which enhanced the damage degree of the wall boundary layer. At the same time, the spiral fin double deflectors can guide the air and reduce the range of heat transfer holes. The heat-exchanged air can be diverted to the upper part of the fin, and the air above the channel can be diverted to the wall to fully exchange heat, resulting in efficient and uniform heat exchange of the heat-exchanged air in the heat exchange channel.

(3) By comparing and analyzing the CTPF of the collector, it can be seen that for a heat exchange channel with a height of 50 mm, the optimum guide vane width and spiral pitch are 16 mm and 160 mm when the fin height and diameter are 38 mm and 25 mm, respectively. The optimum infusion angle is 33.92°.

In this paper, a spiral ribbed collector with deflector is designed to study the enhanced heat transfer characteristics of the collector under the effect of transverse and longitudinal synergistic flow of heat transfer medium under high heat transfer channel, so as to realize efficient and uniform heat transfer. However, the simulation is operated under the condition that the air parameters are constant, and the radiant heat is regarded as a fixed value, and the actual radiation process is extremely complicated, which can be investigated by unsteady state simulation in the future. The collector arrangement is a longitudinal and transverse fork row arrangement, which reduces the number of ribs on the surface of the heat-absorbing plate, and can be further compared with the down-row arrangement in future studies.

Acknowledgment

This work was supported by the China Postdoctoral Science Foundation (Certificate Number: 2023MD734177).

Nomenclature

symbol	Meaning	unit
h	Rib height	mm
d	Thread diameter	mm
w	Width of guide vane	mm
p	Thread pitch	mm
S	Lead	mm
θ	diversion angle	°
ρ	Fluid density	kg/m^3
u，v，w	The velocity components of the fluid in the x, y, and z directions	m/s
p	The static pressure on the micro-clusters	kPa
f_x、f_y、f_z	Energy term caused by resistance	kJ
$\frac{\delta u}{\delta t}$、$\frac{\delta v}{\delta t}$、$\frac{\delta w}{\delta t}$	Unsteady-state term (take 0)	-
C_p	Air-specific heat capacity	J/ (kg • K）
λ	Air thermal conductivity	W/ (m • K)
S	Volume internal heat source	W/m^3
$\frac{\delta T}{\delta t}$	Unsteady-state term (take 0)	-
q	Heat flux per unit area	W/m^2
λ_a	The emissivity of heat-absorbing plate	
δ	Stephen-Boltzmann constant	W/(m²·K^4）

	（5.67×10^{-8}）	
T_1 、T_2	The radiation temperature of the wall surface of the heat-absorbing plate	K

References

[1] Junlong Zou, Yaoguo, ZuoZijian, LiuXi Meng. Employing perforated copper foam to improve the thermal performance of latent thermal energy storage units, *Journal of Energy Storage,72*(2023), pp. 108616.

[2] Mohammad Enamul Hoque, Low Soo-Wah, Mabruk Billah. Time-frequency connectedness and spillover among carbon, climate, and energy futures: Determinants and portfolio risk management implications, *Energy Economics,*2023, pp.107034.

[3] Kaiyin Zhao, Cunqi Jia, Zihao Li, Xiangze Du, Yubei Wang, Jingjing Li, Zechen Yao, Jun Yao. Recent Advances and Future Perspectives in Carbon Capture, Transportation, Utilization, and Storage (CCTUS) Technologies: A Comprehensive Review, *Fuel,351*(2023), pp.128913.

[4] Xun-Qi Chen, Chao-Qun Ma, Yi-Shuai Ren, Yu-Tian Lei. Carbon allowance auction design of China's ETS: A comprehensive hierarchical system based on blockchain, *International Review of Economics & Finance,88*(2023), pp.1003-1019.

[5] K Shahzad, D Abdul, M Umar, A Safi, S Maqsood, A Baseer, B Lu. Analysis of obstacles to adoption of solar energy in emerging economies using spherical fuzzy AHP decision support system: A case of Pakistan, *Energy Reports,10*(2023), pp. 381-395.

[6] Md.Rashid Al-Mamun, Hridoy Roy, Md.Shahinoor Islam, Md.Romzan Ali, Md.Ikram Hossain, Mohamed Aly Saad Aly, Md.Zaved Hossain Khan, Hadi M. Marwani, Aminul Islam, Enamul Haque, Mohammed M. Rahman, Md. Rabiul Awual. State-of-the-art in solar water heating (SWH) systems for sustainable solar energy utilization: A comprehensive review, *Solar Energy,* 2023, pp. 111998.

[7] Jahira Debbarma, Yongrok Choi. A taxonomy of green governance: A qualitative and quantitative analysis towards sustainable development, *Sustainable Cities and Society,79*(2022), pp. 103693.

[8] KC Chang, WM Lin, KM Chung. A lesson learned from the long-term subsidy program for solar water heaters in Taiwan, *Sustainable cities and society,41*(2018), pp. 810-815.

[9] L Yang, N Zhang, Y Yuan, F Haghighat, M Dardir, K Panchabikesan, Q Sun. A double-glazed solar air-phase change material collector for nocturnal heating: Model development and sensitivity analysis, *Energy and Buildings,* 2023, pp. 113070.

[10] Arman Nokhosteen, Sarvenaz Sobhansarbandi. Numerical modeling and experimental cross-validation of a solar thermal collector through an innovative hybrid CFD model, *Renewable Energy,172*(2021), pp. 918-928.

[11] A Kumar, JL Bhagoria, RM Sarviya. Heat transfer and friction correlations for artificially roughened solar air heater duct with discrete W-shaped ribs, *Energy Conversion and management,50*(2009), 8, pp. 2106-2117.

[12] Saini S K, Saini R P. Development of correlations for Nusselt number and friction factor for solar air heater with roughened duct having arc-shaped wire as artificial roughness,

Solar Energy,82(2008), pp.1118-1130.

[13] Bhaumik Modi, Anurag Mudgal, Bansi D. Raja, Vivek Patel. Numerical simulation study on heat collection performance of L-type finned solar flat-plate double-effect collector, *Architecture Science,35*(2019), pp. 79-83.

[14] A Chaube, PK Sahoo, SC Solanki. Analysis of heat transfer augmentation and flow characteristics due to rib roughness over absorber plate of a solar air heater, *Renewable Energy,31*(2006), 3, pp. 317-331.

[15] Yadav A S, Bhagoria J L. A CFD (computational fluid dynamics) based heat transfer and fluid flow analysis of a solar air heater provided with circular transverse wire rib roughness on the absorber plate, *Energy,55*(2013), pp. 1127-1142.

[16] Yadav A S, Bhagoria J L. A numerical investigation of square sectioned transverse rib roughened solar air heater, *International Journal of Thermal Sciences,79*(2014), pp. 111-131.

[17] Tanda G. Heat transfer in rectangular channels with transverse and V-shaped broken ribs, *International Journal of Heat and Mass Transfer,47* (2004), 2, pp. 229-243.

[18] MH Machi, MA Al-Neama, J Buzás, I Farkas. Energy-based performance analysis of a double pass solar air collector integrated to triangular shaped fins, *International Journal of Energy and Environmental Engineering,13*(2022), 1, pp. 219-229.

[19] MS Fahmi, WH Khalil, AJ Shareef. Energy and Exergy Analysis of a Finned-Plate Double Pass Solar Air Heater with Different Arrangement, *Journal of Power and Energy Engineering,8*(2020), 10, pp. 1-17.

[20] Promthaisong P, Eiamsa-Ard S. Fully developed periodic and thermal performance evaluation of a solar air heater channel with wavy-triangular ribs placed on an absorber plate, *International Journal of Thermal Sciences, 140*(2019), pp. 413-428.

[21] Dongxu Jin, Manman Zhang, Ping Wang, Shasha Xu. Numerical investigation of heat transfer and fluid flow in a solar air heater duct with multi V-shaped ribs on the absorber plate, *Energy, 89*(2015), pp.178-190.

[22] AA El-Sebaii, S Aboul-Enein, MRI Ramadan, SM Shalaby, BM Moharram. Thermal performance investigation of double pass-finned plate solar air heater, *Applied energy, 88*(2011), 5, pp. 1727-1739.

[23] S Singh, S Chander, JS Saini. Exergy based analysis of solar air heater having discrete V-down rib roughness on absorber plate, *Energy, 37*(2012), 1, pp.749-758.

[24] Jiang Ping, Xilong Lin，Yuanming Zhang，Xingyang Leng. Structural design and experimental test of V-type perforated plate solar air collector, *Journal of Zhejiang Sci-Tech University (Natural Science Edition), 41*(2019),5, pp. 676-681.

[25] Dengjia Wang, Jin Liu, Yanfeng Liu, Yingying Wang, Bojia Li, Jiaping Liu. Evaluation of the performance of an improved solar air heater with "S" shaped ribs with gap, *Solar Energy, 195*(2020), pp.89-101.

[26] Charles Lhuillier, Pierre Brequigny, Francesco Contino, Christine Mounaïm-Rousselle. Experimental study on ammonia/hydrogen/air combustion in spark ignition engine conditions, *Fuel, 269* (2020), pp.117448.

[27] Kazemipour S, Kabiri-Samani A, Asghari K. Numerical modelling of flow field at shaft spillways with the marguerite-shaped inlets, Proceedings of the Institution of Civil Engineers-Water Management. Emerald Publishing Limited, 2024, pp. 1-12.

[28] Anil Singh Yadav, Om Prakash Shukla, Abhishek Sharma, Irshad Ahmad Khan. CFD analysis of heat transfer performance of ribbed solar air heater, *Materials Today: Proceedings*, *62*(2022), pp. 1413-1419.
[29] Zou Bin. Research on heat transfer mechanism and thermal performance of parabolic trough solar collector, Ph. D. thesis, C Harbin University of Technology, Harbin, China, 2019.
[30] Yunliang Chen, Chao Wu, Bo Wang, Min Du. Three-dimensional numerical simulation of vertical vortex at hydraulic intake, *Procedia Engineering*, *28*(2012), pp. 55-60.
[31] FP Incropera, DP Dewitt. Fundamentals of heat and mass transfer[J]. *Staff General Research Papers*, *27* (2011), 1-2, pp. 139-162.

Received: 30.6.2024.
Corrected: 02.8.2024
Accepted: 17.9.2024.